Opposite Changes Caused by Human Activities in the Occurrence of High Health-Risk Compound Hot-Dry and Hot-Wet Events in China

Haoxin Yao[1], Liang Zhao[2*], Yiling He[3], Wei Dong[4], Xinyong Shen[1*], Jingsong Wang[5,6], Yamin Hu[7], Jian Ling[2], Ziniu Xiao[2] and Cunrui Huang[8*]

[1]Key Laboratory of Meteorological Disaster, Ministry of Education/Joint International Research Laboratory of Climate and Environment Change/Collaborative Innovation Center on Forecast and Evaluation of Meteorological Disasters, Nanjing University of Information Science and Technology, Nanjing 210044, China

[2]State Key Laboratory of Numerical Modeling for Atmosphere Sciences and Geophysical Fluid Dynamics (LASG), Institute of Atmospheric Physics, Chinese Academy of Sciences, Beijing 100029, China

[3]Guangzhou Women and Children's Medical Center, Guangzhou Medical University, Guangzhou 510120, China

[4]Key Laboratory of Geoscience Big Data and Deep Resource of Zhejiang Province, School of Earth Sciences, Zhejiang University, Hangzhou 310058, China

[5]Key Laboratory of Space Weather, National Satellite Meteorological Center (National Center for Space Weather), China Meteorological Administration, Beijing 100081, China

[6]Innovation Center for FengYun Meteorological Satellite (FYSIC), Beijing 100081, China

[7]Guangdong Climate Center, Guangzhou 510640, China

[8]Vanke School of Public Health, Tsinghua University, Beijing 100084, China

Correspondence to: Liang Zhao (zhaol@lasg.iap.ac.cn); Xinyong Shen (shenxy@nuist.edu.cn); Cunrui Huang (huangcunrui@mail.tsinghua.edu.cn)

Table S1. Population, emergency ambulance dispatches, and incidence rates in 13 cities.

Cities	Study duration	Total ambulance dispatches	Annual average ambulance dispatches	Total population (in thousands)	Ambulance incidence rate (per ten thousand population)
Guangzhou	2013-2017	713,537	142,707	1,350.11	105.70
Shenzhen	2015-2016	334,495	167,248	1,137.87	146.98
Zhuhai	2014-2017	125,656	31,414	160.23	196.06
Hangzhou	2014-2018	367,903	73,581	889.20	82.75
Ningbo	2014-2018	99,510	19,902	583.78	34.09
Taizhou	2016-2018	108,338	36,113	597.10	60.48
Zhoushan	2014-2018	107,804	21,561	114.60	188.14
Lishui	2014-2018	32,394	8,099	266.38	30.40
Zhenzhou	2017-2019	269,744	89,915	1,013.60	88.71
Luoyang	2014-2016	52,788	17,596	688.85	25.54
Xuchang	2017-2019	35,964	11,988	446.21	26.84
Jinan	2014-2017	192,271	48,068	621.61	77.33
Huairou	2016-2018	17,377	5,792	41.40	139.90
Total	/	2,457,781	673,984	7,910.94	/

Table S2. Basic information of the 10 CMIP6 models and ERA5 reanalysis used in this study.

Models	Time period	ALL	NAT	Horizontal Resolution (lat × lon)
ACCESS-CM2	1979-2014	√	√	1.25 × 1.675
ACCESS-ESM1-5	1979-2014	√	√	1.25 × 1.875
CanESM5	1979-2100	√	√	2.81 × 2.81
CESM2	1979-2014	√	√	0.9424 × 1.25
FGOALS-g3	1979-2014	√	√	2.00 × 2.30
GFDL-ESM4	1979-2014	√	√	1.25 × 1.00
IPSL-CM6A-LR	1979-2014	√	√	1.2676 × 2.5
MIROC6	1979-2100	√	√	1.41 × 1.41
MRI-ESM2-0	1979-2014	√	√	1.124 × 1.125
NorESM2-LM	1979-2014	√	√	1.895 × 2.5
ERA5 Reanalysis	1979-2022	/	/	0.25 × 0.25

Analysis of health risks and the definition of high health-risk temperature and relative humidity thresholds.

Through identifying vulnerability during extreme temperature exposure periods, this study discovered that individuals aged 60 and above are susceptible to illness due to high temperatures. Previous assessments of temperature-related emergency risks have also highlighted the heightened vulnerability of the elderly during periods of high heat. This susceptibility may stem from diminished thermoregulatory capacity and the presence of underlying chronic illnesses among the elderly population, rendering them more sensitive to temperature fluctuations.

Furthermore, the study found that individuals aged 18-44 are particularly sensitive to temperature exposure. This sensitivity could be attributed to their status as working-age individuals, who are more likely to experience higher levels of heat exposure compared to other age groups. For instance, they may engage in outdoor occupations such as agriculture and construction, thereby increasing their exposure to high temperatures.

Additionally, the research revealed a significant increase in the risk of workplace injuries during periods of high temperatures. Despite the working-age population generally possessing higher thermoregulatory capacity and heat tolerance compared to the elderly or children, the heightened risk of workplace injuries during high temperatures renders this age group more susceptible during such periods.

Moreover, the study identified a significant increase in the risk of dizziness during extreme temperature exposure periods. Dizziness encompasses symptoms or signs such as heat exhaustion, dizziness, and fatigue. While these symptoms are non-lethal, failure to promptly address them can pose serious threats to life.

Currently, assessments of temperature-related health risks often oversimplify complex environmental exposures by assuming that a single temperature index sufficiently reflects external environmental conditions, thereby leading to inaccuracies in health risk assessments.

Therefore, this study evaluated compound weather conditions to provide a more accurate assessment of temperature-related health risks. The following steps outline this process (Figure S1):

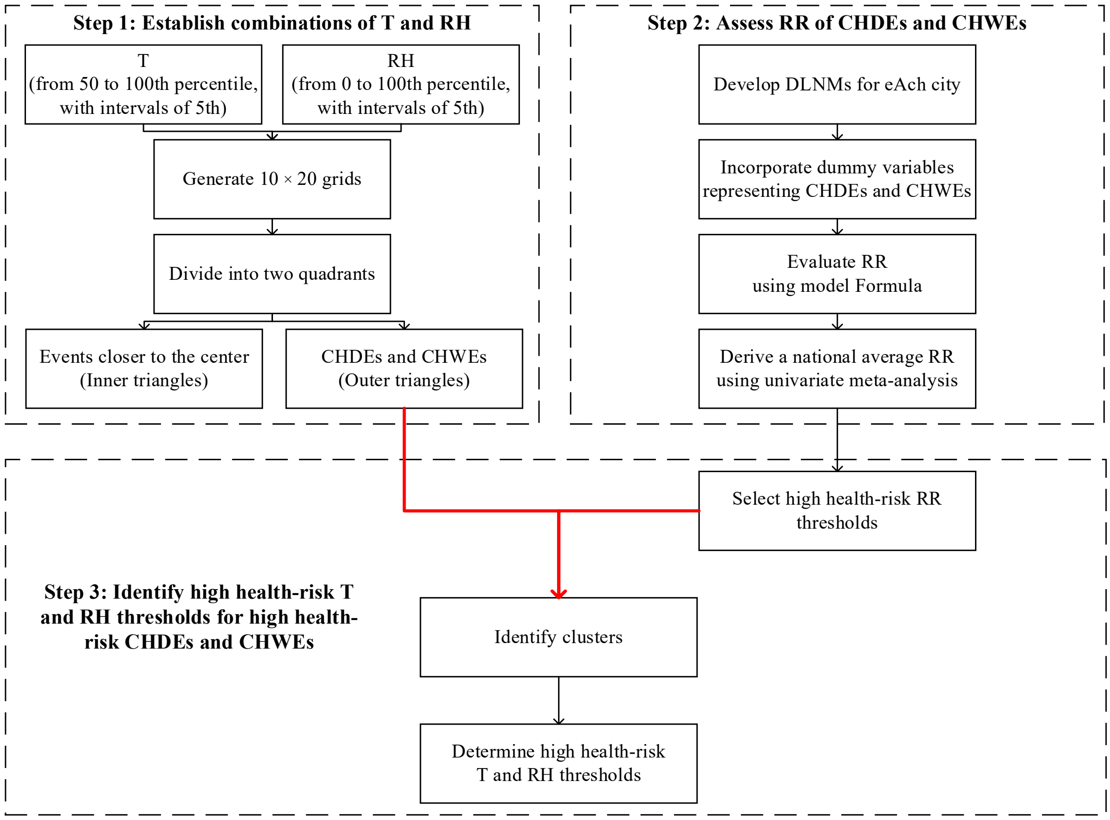

Figure S1. The process diagram for identifying T and RH thresholds for high health-risk CHDEs and CHWEs.

The specific explanation of the process diagram is as follows:

Step1: Establish combinations of T and RH.

Combine T (from 50th to 100th percentile, with intervals of 5th) with RH (from 0 to 100th percentile, with intervals of 5th) to create a 10 × 20 square grid. Use the 50th percentile of RH to divide the grid into two quadrants, corresponding to high-T high-RH events and high-T low-RH events. Furthermore, within each quadrant, connect the RH corresponding to the 50th percentile with the relative T using line segments. This results in two quadrants, each divided into an outer triangle, representing events further from the center of the square, and an inner triangle, representing events closer to the center. The outer triangle represents CHDEs and CHWEs.

Step 2: Assessing the RR of CHDEs and CHWEs.

Developing Distributed Lag Non-Linear Models (DLNMs) for the RR associated with each city and exposure intensity of CHDEs and CHWEs. Incorporate dummy variables representing CHDEs and CHWEs, with dates of CHDEs and CHWEs set to 1 and the rest to 0. Evaluate the emergency risk of CHDEs and CHWEs using the following model formula:

$$logE[Y_t] = \alpha + cb(HE_t, L) + NS(time, df) + \beta_1 DOW_t + \beta_2 H_t$$

Here, t represents the observed day, Y_t denotes the number of emergency dispatches on day t, α is the intercept, and HE_t indicates whether day t is an exposure event for CHDEs and CHWEs, where 0 indicates a non-exposure event, while 1 indicates CHDEs and CHWEs exposure. cb is the cross-matrix established for daily compound exposure events and the maximum lag days (L). NS represents the natural cubic spline function, and df denotes degrees of freedom, determined based on the Akaike Information Criterion (AIC), selecting the model with the minimum AIC for corresponding degrees of freedom. $time$ controls for the long-term trend and seasonal trends, $\beta_1 DOW_t$ represents the day of the week variable, and $\beta_2 H_t$ is a binary variable reflecting whether it's a holiday.

To estimate the overall population RR during exposure events for different CHDEs and CHWEs across 13 cities, a univariate meta-analysis is conducted. This involves combining effect sizes to derive a national average RR during exposure events for each CHDE and CHWE.

Step 3: Identify T and RH thresholds for high health-risk CHDEs and CHWEs.

Arrange the RR of all combinations of CHDEs and CHWEs exposure events in ascending order. Select the RR value corresponding to the 80th percentile as the high health-risk RR threshold. In exposure events of CHDEs and CHWEs, identify clusters of high health-risk CHDEs and CHWEs to obtain T and RH values closest to the 50th percentile.

For instance, in the case of CHDEs exposure events, identify clusters of high health-risk-T and high health-risk-RH events. The minimum T and minimum RH values within these clusters are considered the T and RH thresholds for high health-risk CHDEs.

Table S3. The high health-risk CHDEs' RR in China and 13 cities (T ≥ 80th percentile & RH ≤ 10th percentile).

	CHDEs (T ⩾ 80th percentile & RH ⩽ 10th percentile)	
Cities	RR	95%CI
Guangzhou	1.101	[0.967,1.254]
Shenzhen	1.083	[0.996,1.178]
Zhuhai	1.007	[0.933,1.087]
Hangzhou	1.275	[1.033,1.575]
Taizhou	1.119	[0.902,1.388]
Ningbo	1.069	[0.961,1.190]
Lishui	1.339	[1.001,1.792]
Zhoushan	1.171	[0.998,1.374]
Jinan	1.155	[1.030,1.295]
Zhengzhou	1.193	[1.049,1.357]
Luoyang	1.042	[0.897,1.211]
Xuchang	1.076	[0.909,1.274]

Huairou	0.831	[0.358,0.931]
Average	**1.112**	**[0.926,1.300]**

Table S4. Same as Table S3, but for high health-risk CHWEs (T ≥ 90th percentile & RH ≥ 55th percentile & RH ≥ 70%).

	CHWEs (T ⩾ 90th percentile & RH ⩾ 55th percentile & RH ⩾ 70%)	
Cities	RR	95%CI
Guangzhou	1.085	[1.011,1.164]
Shenzhen	1.052	[0.994,1.113]
Zhuhai	1.190	[1.026,1.381]
Hangzhou	1.154	[0.995,1.339]
Taizhou	0.977	[0.892,1.070]
Ningbo	1.168	[0.930,1.467]
Lishui	1.153	[1.042,1.276]
Zhoushan	1.809	[0.810,4.042]
Jinan	1.120	[1.067,1.176]
Zhengzhou	1.075	[1.026,1.126]
Luoyang	1.133	[1.001,1.282]
Xuchang	1.196	[1.060,1.349]
Huairou	1.151	[0.989,1.340]
Average	**1.174**	**[0.988,1.471]**

Table S5. Same as Table S3, but for single high-T Events (T ≥ 90th percentile).

	Single high-T Events (T ⩾ 90th percentile)	
Cities	RR	95%CI
Guangzhou	1.045	[1.027,1.064]
Shenzhen	1.091	[1.054,1.130]
Zhuhai	1.081	[1.028,1.137]
Hangzhou	1.064	[1.025,1.105]
Taizhou	1.029	[0.980,1.080]
Ningbo	1.068	[1.015,1.124]
Lishui	1.205	[1.102,1.318]
Zhoushan	1.221	[1.110,1.343]
Jinan	1.096	[1.048,1.147]
Zhengzhou	1.053	[1.013,1.095]
Luoyang	1.064	[0.986,1.148]

Xuchang	1.202	[1.092,1.323]
Huairou	1.094	[0.962,1.245]
Average	**1.101**	**[1.034,1.174]**

Table S6. Same as Table S3, but for single high-T events (T $\geqslant$ 80th percentile).

	Single high-T events (T $\geqslant$ 80th percentile)	
Cities	RR	95%CI
Guangzhou	1.077	[1.052,1.096]
Shenzhen	1.087	[1.056,1.119]
Zhuhai	1.075	[1.037,1.114]
Hangzhou	1.081	[1.036,1.128]
Taizhou	1.123	[1.058,1.192]
Ningbo	1.114	[1.054,1.178]
Lishui	1.128	[1.041,1.223]
Zhoushan	1.163	[1.073,1.261]
Jinan	1.136	[1.080,1.195]
Zhengzhou	1.059	[1.023,1.097]
Luoyang	0.999	[0.950,1.051]
Xuchang	1.126	[1.024.1.238]
Huairou	1.052	[0.973.1.137]
Average	**1.094**	**[1.035,1.156]**

The World Meteorological Organization (WMO) notes that as of 2021, there is no universally accepted definition of threshold values for compound events (WMO, 2021; Miao et al., 2024). In meteorology, there exists a variety of proposed definitions, metrics, and indices for these events. Previous research has utilized specific relative thresholds, such as the 10th and 90th percentiles (alternatively, 25th and 75th percentiles), to denote the thresholds for compound events defined based on the combination of temperature and humidity (Wang et al., 2020; Aihaiti et al., 2021; Peng et al., 2023; Lin et al., 2024).

WMO. WMO Atlas of Mortality and Economic Losses from Weather, Climate and Water Extremes (1970–2019) (WMO, 2021).

Miao, L., Ju, L., Sun, S. et al. (2024). Unveiling the dynamics of sequential extreme precipitation-heatwave compounds in China. *npj Clim Atmos Sci*, 7(67). https://doi.org/10.1038/s41612-024-00613-5

Peng, T., Zhao, L., Zhang, L., Shen, X., Ding, Y., Wang, J., Li, Q., Liu, Y., Hu, Y., Ling, J., Li, Z., & Huang, C. (2023). Changes in Temperature-Precipitation Compound Extreme Events in China During the Past 119 Years. *Earth and Space Science*, 10. https://doi.org/10.1029/2022EA002777

Aihaiti, Ailiyaer, Zhihong Jiang, Lianhua Zhu, Wei Li and Qinglong You. (2021). Risk changes of compound temperature and precipitation extremes in China under 1.5 °C and 2°C global warming. *Atmospheric Research*, 264, 105838. https://doi.org/10.1016/j.atmosres.2021.105838

Wang, J., Feng, J., Yan, Z., & Chen, Y. (2020). Future Risks of Unprecedented Compound Heat Waves Over Three Vast Urban Agglomerations in China. *Earth's Future*, 8. https://doi.org/10.1029/2020EF001716

Lin, X., Wang, Y., & Song, L. (2024). Urbanization Amplified Compound Hot Extremes Over the Three Major Urban Agglomerations in China. *Geophysical Research Letters*. https://doi.org/10.1029/2023GL106644

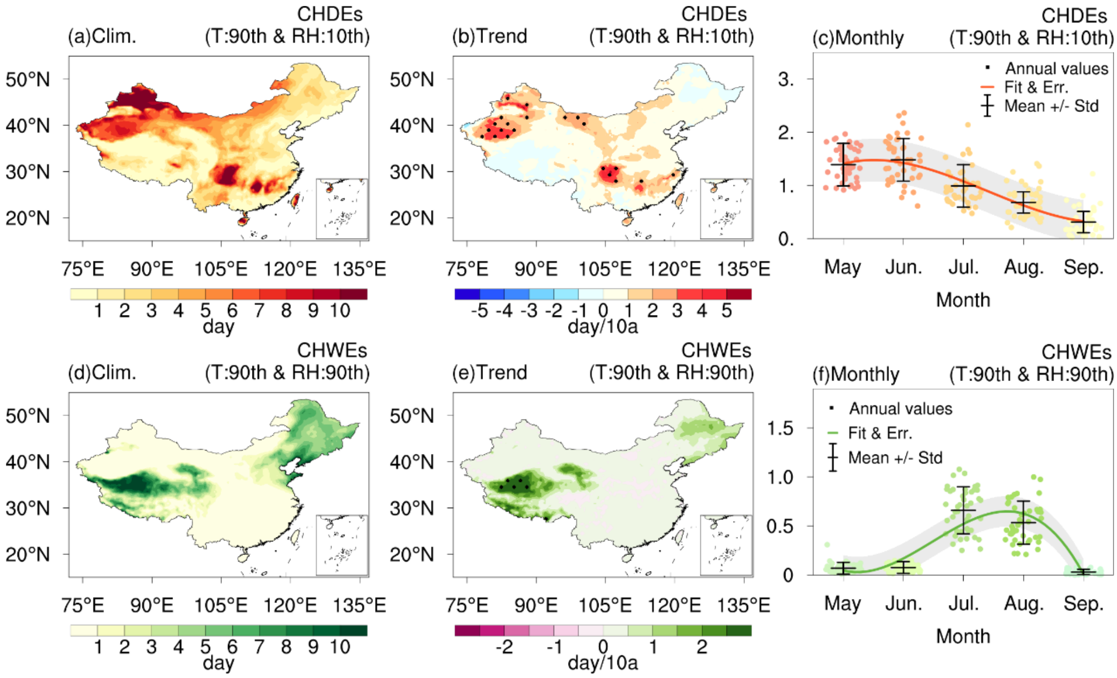

Figure S2. Climatology (units: d) of the frequency of (a) CHDEs (T ≥90th percentile & RH ≤ 10th percentile) and (d) CHWEs (T ≥90th percentile & RH ≥ 90th percentile) during 1979−2022 based on ERA5. Linear trends (units: day/10a) in the frequency of (b) CHDEs and (e) CHWEs for (a, d) observations. The frequency of (c) CHDEs and (f) CHWEs across the Chinese region from May to September each year. The dotted area indicates that the linear trend is significant at the 95% confidence level.

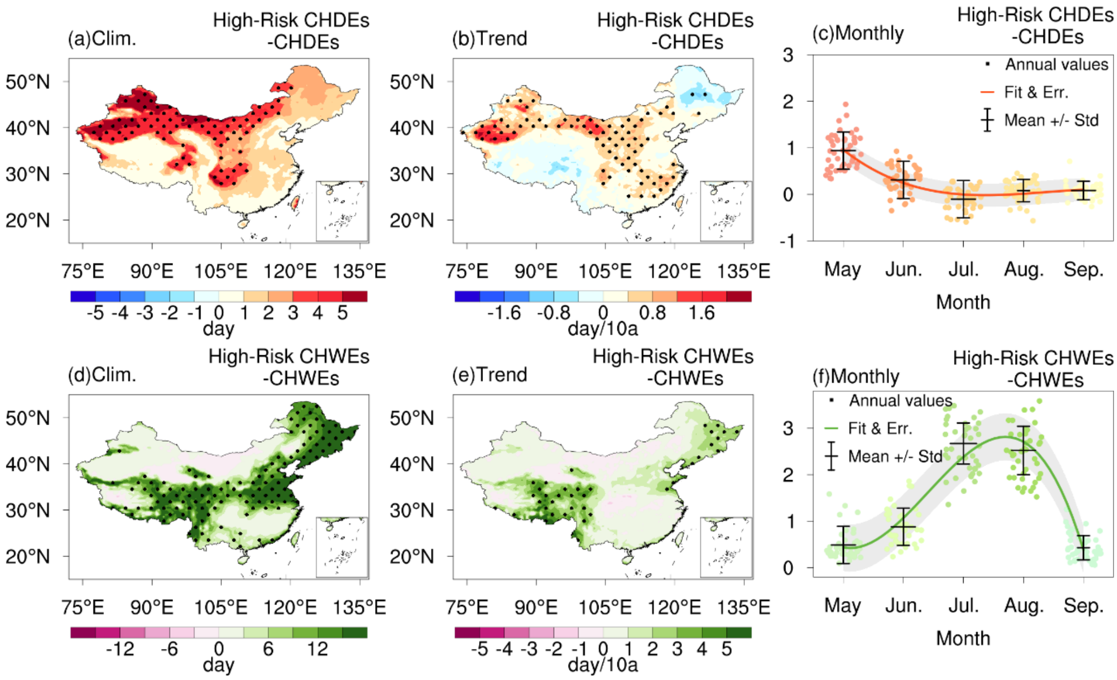

Figure S3. Same as the upper panels illustrates the difference between high health-risk CHDEs (T ≥ 80th percentile & RH ≤ 10th percentile) and CHDEs (T ≥ 90th percentile & RH ≤ 10th percentile). The lower panels represent the difference between high health-risk CHWEs (T ≥ 25th percentile & RH ≤ 55th percentile & RH ≥ 70%) and CHWEs (T ≥ 90th percentile & RH ≥ 90th percentile).

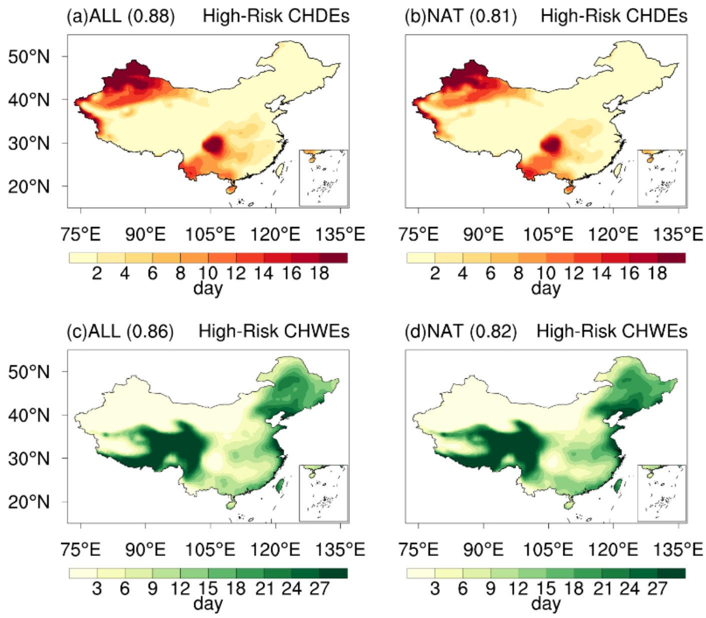

Figure S4. Multi-model ensemble averages of CMIP6 data for 1979-2014: (a) high health-risk CHDEs and (c) high health-risk CHWEs under ALL Simulations. (b, d) Same as (a, c), but for NAT Simulations. The numerical values in the top left of panels are the spatial correlations between observations and simulations.

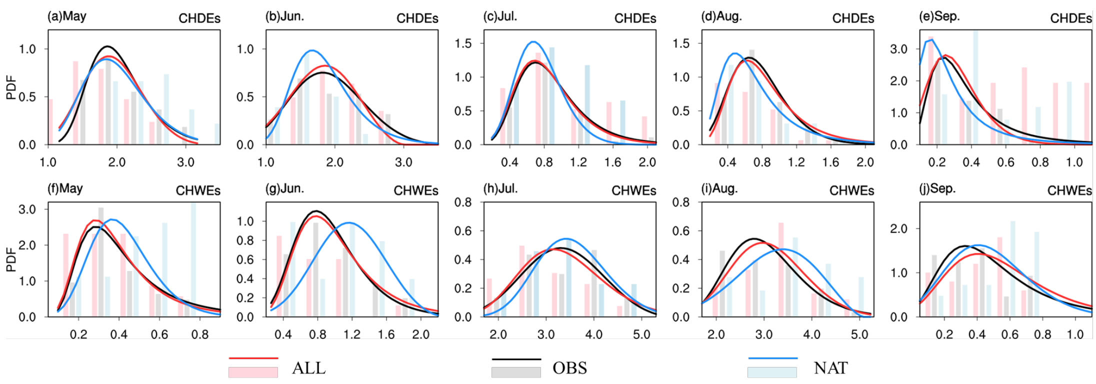

Figure S5. Original (bar) and GEV fitted PDFs (solid line) of observations (gray bar and black line) and ALL simulations (pink bar and red line) and NAT simulations (light blue bar and blue line) from May to September for high health-risk CHDEs (upper panels) and high health-risk CHWEs (lower panels).

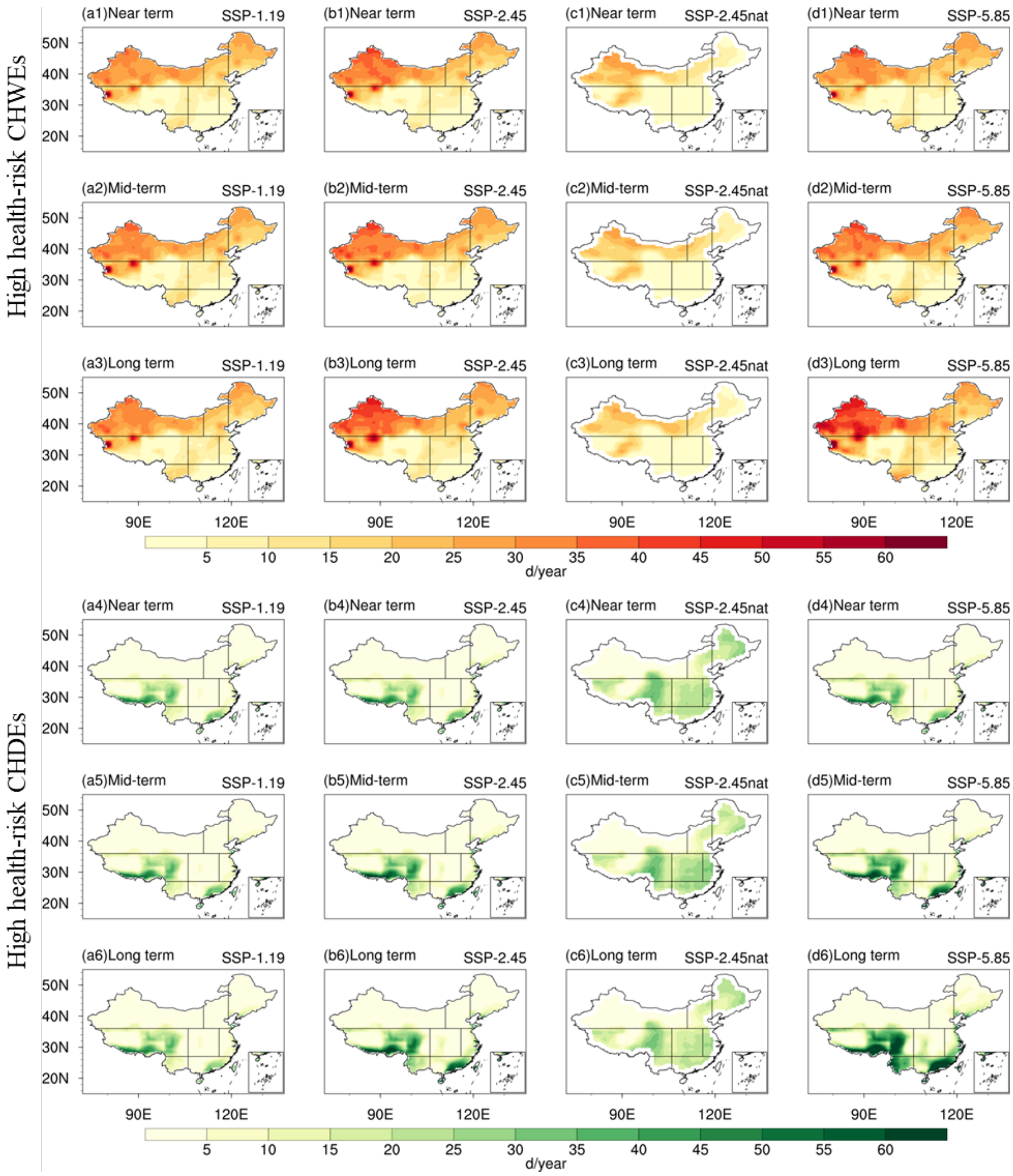

Figure S6. The spatial distribution of the average occurrence frequency (units: d/year) of high health-risk CHDEs and high health-risk CHWEs over near term (2021-2040), mid-term (2041-2060), and long term (2081-2100) periods. The data are calculated from the CMIP6 multi-model ensembles, analyzed under four scenarios: (a) SSP1-1.9, (b) SSP2-4.5, (c) SSP2-4.5nat, and (d) SSP5-8.5. High health-risk CHDEs are represented by indices 1-3, while high health-risk CHWEs are represented by indices 4-6.